LAWRENCE
LIVERMORE
NATIONAL
LABORATORY

UCRL-CONF-214524

First Laser-Plasma Interaction and Hohlraum Experiments on NIF

E. L. Dewald, S. H. Glenzer, O. L. Landen, L. J. Suter, O. S Jones, J. Schein, D. Froula, L. Divol, K. Campbell, M. S. Schneider, J. W. McDonald, C. Niemann, A. J. Mackinnon

August 10, 2005

32nd EPS Conference on Plasma Physics
Tarragona, Spain
June 26, 2005 through July 1, 2005

First Laser-Plasma Interaction and Hohlraum Experiments on NIF

E.L. Dewald, S.H. Glenzer, O.L. Landen, L.J. Suter, O.S. Jones, J. Schein, D. Froula, L. Divol, K. Campbell, M.S. Schneider, J.W. McDonald, C. Niemann, A.J. Mackinnon

LLNL, P.O. Box 808, Livermore, CA 94550

Abstract
Recently the first hohlraum experiments have been performed at the National Ignition Facility (NIF) in support of indirect drive Inertial Confinement Fusion (ICF) designs. The effects of laser beam smoothing by spectral dispersion (SSD) and polarization smoothing (PS) on the beam propagation in long scale gas-filled pipes has been studied at plasma scales as found in indirect drive gas filled ignition hohlraum designs. The long scale gas-filled target experiments have shown propagation over 7 mm of dense plasma without filamentation and beam break up when using full laser smoothing. Vacuum hohlraums have been irradiated with laser powers up to 6 TW, 1-9 ns pulse lengths and energies up to 17 kJ to activate several diagnostics, to study the hohlraum radiation temperature scaling with the laser power and hohlraum size, and to make contact with hohlraum experiments performed at the NOVA and Omega laser facilities. Subsequently, novel long laser pulse hohlraum experiments have tested models of hohlraum plasma filling and long pulse hohlraum radiation production. The validity of the plasma filling assessment in analytical models and in LASNEX calculations has been proven for the first time.. The comparison of these results with modeling will be discussed.

1. Introduction

In present indirect drive Inertial Confinement Fusion designs the fuel capsule is placed inside a high-Z hohlraum. The hohlraum interior converts the drive laser beams into soft x-rays that are used to compress the capsule and drive it to ignition and burn. In the ICF design the high-Z hohlraums contain a mid-to-low Z fill to slow down the hohlraum wall plasma that may otherwise compromise capsule compression symmetry and hinder ignition. The success of fuel capsule ignition depends on a variety of aspects including hohlraum energetics, capsule compression symmetry control and shock timing used to efficiently compress the capsule. The optimization of hohlraum energetics deals with the laser propagation and absorption in the hohlraum, the conversion efficiency from laser energy into soft x-rays and minimization of x-ray radiation losses in the hohlraum walls and laser entrance holes (LEH).

The National Ignition Facility (NIF) that is currently under construction [10] is a 192 laser beam system that is designed to deliver up to 1.8 MJ of energy at a wavelength of λ_0 = 351 nm. The laser is designed to first achieve indirect drive ICF and will also be used for a variety of High Energy Density (HED) experiments. After the first available four NIF laser beams forming the so-called quad 31B were successfully activated, the first experiments were recently performed. In this paper we will present results from the first hohlraum energetics related Laser-Plasma Interaction (LPI) and vacuum hohlraum experiments performed on NIF.

The main purpose of the performed LPI experiments is to study the effect of laser beam smoothing on laser propagation in gaseous long, ignition scale plasmas. Several smoothing techniques such as the use of phase plates (CPP), polarization smoothing (PS) and high frequency temporal smoothing (SSD) were used to achieve a uniform laser intensity profile. (references)

The vacuum hohlraum experiments were designed to activate several hohlraum drive diagnostics and to make connection with hohlraum database obtained at the NOVA and Omega laser facilities. Furthermore, using the unique capability of the NIF laser to deliver long high energy pulses of up to 20 ns in length, models of extreme hohlraum plasma filling were corroborated. These models are used to predict the hohlraum radiation limits as a function of laser power and pulse length that are important for designing High Energy Density HED physics experiments.

2. Experiments

Figure 1 shows the experimental layout used in these experiments. For the LPI experiments the laser beams are propagated in up to ignition hohlraum relevant 7 mm-long CO2-filled CH gas pipes. The four NIF laser beams enter the targets on the axis forming effectively an f/8 beam. The beam best focus of 0.5 mm is placed in the target center. For a total laser energy of 16 kJ in a flattop pulse with 3.5 ns length, intensities up to 2×10^{15} W/cm^2 are reached in the plasma. The laser propagation is inferred from laser plasma emission measured side-on with a gated multi-framing x-ray camera filtered for 3.5 keV (> 3 keV?) radiation. The laser energy backscattered inside and within 20°? of the laser final focusing lenses was measured with a Full Aperture Backscattering

Station (FABS) and a Near Backscattering Imager (NBI) respectively..(references) Streak cameras connected to spectrometers in FABS measure time and spectrally resolved stimulated Brillouin and Raman Backscattering Spectra (SBS, SRS).

The laser propagation and backscattering is measured as a function of beam smoothing. To understand the created plasma conditions and the beam propagation the experiments were coupled with 3-dimentional pf3d and 2-dimensional LASNEX simulations. The cell size used in LASNEX simulations is of several μm and the laser beams are simulated by ray tracing. The used laser intensity profile idealized. Therefore pf3d is used in addition to LASNEX to understand the beam propagation. The cell size in pf3d is in the order of the laser wavelength allowing us to simulate laser beam refraction and the effect of the ponderomotive force on the created plasma electrons. Furthermore, a realistic beam profile with the experimentally measured CPP phase plate profiles is used. Since unlike LASNEX pf3d does not have a radiation absorption option, both types of simulations are employed.

For the vacuum hohlraum experiments we used cylindrical Au hohlraums of various sizes with a single LEH The hohlraum back wall is irradiated with the four laser beams effectively forming an f/8 cone that propagates along the hohlraum axis (see Fig. 1). Full aperture phase plates [12] and polarization smoothing [13] were installed on the laser beams providing a uniform intensity profile spot with a radial profile that is approximated by a n = 5 super-Gaussian with a 500 μm diameter (1/e points) with best focus placed at the LEH [11]. Constant power (flattop) laser pulses with 100 ps rise and fall times were used with energies between 5 and 17 kJ and pulse lengths between 2 and 9 ns. Several hohlraum sizes were employed between scales 3/4 (1.2 mm diameter, 1.1 mm long) and 3/2 (2.4 mm diameter, 2.3 mm long). All Au hohlraum walls were 5 μm thick, backed by a 100 μm CH coating, allowing us to measure spatially resolved Au L-shell emission (> 9 keV) and to infer the hohlraum plasma fill dynamics [14]. In these experiments the gated framing camera was filtered for photon energies > 6 keV with 100 μm Al, however when viewing side-on through the 5μm thick hohlraum Au walls the total filtering transmits > 9 keV x rays.

During these first hohlraum experiments on NIF the hohlraum drive diagnostics capability including Dante and hot electron production were activated (Fig. 1). The

hohlraum radiation temperature was measured with temporal and spectral resolution through the LEH at 21.6° with an 18-channel absolutely calibrated soft x-ray power diagnostic, Dante [15]. Dante has a partial view of the initial laser spots on the hohlraum back wall and provides a measure of the radiation flux that includes both the primary laser-plasma emission and the re-emitting walls. The hot electron production inside the hohlraum was inferred from 20-100 keV absolutely calibrated x-ray spectra of the electron bremsstrahlung emission [18] spectrally resolved with 8 channels. Similar to the LPI experiments, the total backscattered laser energy was measured with FABS and NBI. A static x-ray imager (SXI) confirmed that the beams propagate through the LEH without striking the outside walls of the hohlraum.

A series of experiments using 2 ns flattop pulses and variable laser energy in the 5-13 kJ range was first performed to measure the radiation temperature scaling with laser power and hohlraum size, ranging between scale 3/4 and scale 1, in a regime similar to previous hohlraums [8,9,19] where minimal plasma filling is expected. Hohlraum plasma filling was studied for longer laser pulses of 6 and 9 ns with up to 17 kJ energy in larger scale 1 to 3/2 hohlraums. The thin wall imaging and Dante measurements were compared to 2-dimensional LASNEX radiation-hydrodynamics simulations.

3. Results and discussion

3.1 LPI experiments

Laser propagation in 7 mm long CO_2 plasma and laser backscattering were compared for laser beam smoothing using CPP, SSD and PS to using CPP only. Enhanced plasma filammentation and laser beam spraying when using only CPP were inferred from 3.5 keV plasma emission. The additional smoothing given by SSD and PS suppresses plasma filamentation and beam spraying. Plasma formation and beam propagation was simulated using LASNEX. The time history of the post-processed 3.5 keV emission agrees well with the measured x-ray images obtained when using CPP, SSD and PS as shown in Figure 2. According to both LASNEX and pf3d simulations, a relatively flat axial profile of electron temperature of 2 keV is reached by laser heating at electron densities of 8% n_c where n_c [cm^{-3}]= 1.1 10^{21} /λ^2[μm^2] is the critical density at the laser wavelength used. The backscattering measurements have shown that the backscattered

light is mainly SBS. Moreover, the NBI images (Figure 3) show that the laser is backscattered under a smaller solid angle when using CPP, SSD and PS for beam smoothing compared to when using CPP only. Specifically, when using additional smoothing with SSD and PS the laser is mainly backscattered in the lens cone, while when using DPP only the laser energy is backscattered mainly outside the laser focusing lens. This confirms the reduced laser beam spraying when using additional beam smoothing by SSD and PS inferred from the gated x-ray images (Figure 2). Similar to previous experiments performed on NOVA and Omega laser facilities (reference) the total laser backscattering was reduced when using additional smoothing by SSD and PS. In the pf3d simulations for the CPP only case, the laser is backscattered under a smaller angle than it was measured with NBI (Fig. 3b and c) (needs line-out in simulation to prove statement).

3.2 Vacuum hohlraum experiments

For all vacuum hohlraum experiments performed at intensities up to $3x10^{15}$ W/cm^2 the laser backscattering was negligible for both SRS (<0.05%) and SBS (0.6%). These backscattering values were roughly one order of magnitude smaller than those measured in hohlraum experiments performed at the Nova laser facilities at similar laser intensities, spatial beam smoothing, and peak hohlraum radiation temperatures. (reference Novavacuum paper with KPP)) This may be due to Nova/ and NIF vacuum hohlraums being irradiated by beams incident at 40° vs normal to the hohlraum wall, , leading to shorter effective scalelengths, higher flow gradients, and hence lower laser-plasma instability gain-length products for the NIF-case. Figure 4 shows hot electron data for all vacuum hohlraum experiments on NIF. Similar to laser backscattering the measured hot electron fraction was <~1% in all hohlraums except the smallest, scale-¾ hohlraum where it was 4%. The measurements show that the hot electron fraction increases with the laser power and for smaller hohlraums. The hot electron temperature was 30 keV.

3.2.1 Hohlraum power scaling

The time resolved absolute flux spectra over a wide range of hohlraum temperatures were recorded with Dante and post-processed from LASNEX simulations. Figure 5 shows

typical spectra recorded on the peak of the drive for two different hohlraum temperatures and postprocessed from LASNEX simulations, showing good agreement. The spectra have a Planckian shape with enhanced emission in the 4-3 Au M-band and 4-4 N-band spectral ranges. A series of experiments using 2 ns flattop pulses and variable laser energy in the 5-13 kJ range was performed to measure the radiation temperature scaling with laser power and hohlraum size under conditions where minimal plasma filling is expected. Figure 6a shows measured and predicted radiation temperatures for scale-1 (1.6 mm diameter, 1.5 mm long) and scale-3/4 (1.2 mm diameter, 1.1 mm long) hohlraums with a LEH size of 0.75 of the hohlraum diameter as well as the Dante view of the target and laser spots. We find that the radiation temperature scales as expected with both the laser power and hohlraum size from detailed LASNEX simulations [17] and from analytical scaling laws [18]. The peak radiation temperature between Dante data and LASNEX calculations agree within the experimental Dante radiation temperature error bar of 2 %. Figures 6b and c show thin wall images at the end of the 2 ns pulse for a scale-1 and scale-3/4 hohlraum experiments conducted at the same laser power of 6.7 TW. In the scale-1 hohlraums the emission is localized at the back wall, confirming expectations of no plasma filling. The smaller scale-3/4 hohlraum also shows bright emission from the back wall and some volume emission indicating that laser absorption by inverse bremsstrahlung in the LEH region becomes important at the end of the experiment.

3.2.2 Long pulse hohlraums

Scale 1 and 1.5 hohlraums were heated by 6 and 9 ns long pulses to test hohlraum radiation production limits due to plasma filling. Figure 7 shows that when irradiated by a longer 6 ns laser pulse the Au L-shell emission in the LEH region for a scale-1 hohlraum (0.8 mm LEH) eventually dominates as a result of plasma filling. We apply LASNEX simulations to calculate the ablation from the gold hohlraum walls by soft x-rays and the cylindrically inward motion of the ablated plasma. First, the low-density ablation plasma moves into the beams path and is directly heated by the laser beams. This creates a high plasma pressure on the hohlraum axis retarding complete closure of the hohlraum, which is an important part of the hydrodynamics (Fig. 7 at 1 ns). Second,

roll-over of the internal radiation temperature occurs at ~ 4 ns when the ablated plasma moving inward from the LEH begins to significantly absorb and refract the beam at the LEH. By the end of the laser pulse the LEH plasma completely absorbs the laser beams. As a consequence, the hard x-ray radiation production migrates from the hohlraum back wall to the region of the LEH. This behavior is well reproduced by LASNEX post processed calculations of the Au L-shell emission (Fig. 7b) particularly the sudden transition from back wall to LEH dominated emission at ~ 4ns.

In addition to the scale-1 hohlraum irradiated with a 6 ns laser pulse, we performed long pulse experiments using larger, scale-3/2 hohlraums (2.4 mm diameter, 2.25 mm long, 1.4 mm LEH) demonstrating that our LASNEX modeling correctly predicts the size scaling of plasma fill limits and the roll-over of the internal radiation temperature. With the same 6 ns laser pulse into the larger scale-3/2 hohlraum, the Au L-shell emission remains considerably stronger at the back wall than at the LEH, indicating that the hohlraum fill plasma density is moderate and that the laser still propagates into the hohlraum until the end of the laser pulse. However, when irradiating the same scale-3/2 hohlraum with a longer, 9 ns laser pulse of similar energy, we observe strong emission in the LEH starting at t = 7 ns.

Figure 8 shows the radiation temperature through the LEH T_{LEH} for the long pulse experiments measured by Dante, and simulated by LASNEX and the corresponding gated thin wall images. Figure 8 also shows the corresponding measured and simulated "M-band flux" (radiation > 2keV). Both the 9 ns scale-3/2 and the 6 ns scale-1 results (b and c) show two characteristic signatures of roll-over not seen in the 6 ns scale-3/2 result (a). Most prominent is the rise in Au M-band flux. These > 2 keV x-rays are produced by the dense LEH plasma that absorbs the laser beams and that is located where its emission is fully visible by Dante. In order to infer a roll-over time τ from our experiments, we use the time of the sudden rise in Au M-band flux. Less prominent is a sudden rise in T_{LEH} that occurs when the LEH plasma becomes dense enough to entirely stop the laser beams. Further, Fig. 8 shows the calculated "internal T_R ", which is the radiation temperature that would drive an HED package located inside the hohlraum. This calculation shows "roll-over" at the time τ (Fig. 8b and c) when the LEH plasma is dense enough to absorb entirely the laser energy, coincident with the sudden rise in M-band emission, the rise in

LEH temperature and the migration of the L-shell emission from the back wall to the LEH.

3.2.3 Analytical model of plasma filling

In addition to detailed numerical simulations, these results can be understood and extrapolated to higher laser energies and powers by applying a simple analytic model for radiation temperature limits [ ]. This model is based on the increased hydrodynamic losses and thin coronal radiative losses proportional to n_e^2 (n_e-electron density) [17] that occur when the laser absorption region migrates to the LEH as the hohlraum fills with plasma, leading to the roll-over in the internal radiation temperature. In our model these losses become important at the LEH when the inverse bremsstrahlung absorption length in the laser heated LEH plasma becomes shorter than the LEH radius. The plasma conditions for inverse bremmstrahlung are calculated by balancing x-ray ablated plasma pressure with laser heated plasma pressure and balancing heat conduction losses with inverse bremmstrahlung heating [ ].

The model also uses a traditional hohlraum power balance omitting thermal radiation losses out of the LEH which are lower than wall losses for the LEH sizes used here. A constant x-ray conversion efficiency (C.E.) of 75% and 100% absorbed laser energy are assumed, the later motivated by the very low values of measured laser backscattering. The model gives the roll-over radiation temperature $T_{max}=T_R(\tau)$ in terms of laser power, roll-over time τ and LEH radius r:

$$T_{max} = 1.0 P_L^{0.20}/r^{0.20}\tau^{0.07} = 1.0 E_L^{0.20}/r^{0.20}\,\tau^{0.27} \qquad (1)$$

where T_{max} is in heV units, the flattop laser power (energy) P_L (E_L) is in TW (kJ), the filling time τ is in ns and the LEH radius r is in cm. The middle expression in Eq. (1) is applicable when the laser is power limited and the (right-hand) expression is applicable when the pulse length is long enough that the laser is energy limited. The optimum hohlraum size at fixed laser power decreases for shorter fill (roll-over) times τ as smaller hohlraums get hotter and fill faster with plasma.

As shown in Fig. 8, the simulated Dante (T_{LEH}) and internal (T_R) temperatures have similar values at the roll-over time, which allows us to compare T_{max} (Eq. (1)) directly to the measured Dante temperature (T_{LEH}). Figure 9 plots the experimental Dante

temperatures (full circles) at the fill times τ and the corresponding T_{max} limits calculated with Eq. (1) (crosses) showing good agreement. Included are data points for the scale ¾ (Fig. 6a and c) which showed significant LEH emission at the end of the pulse and for a smaller scale-3/8 hohlraum, heated by a 1.1 ns laser pulse [24].

Figure 9 also shows analytical curves that describe the T_R limits (Eq. (1)) imposed by plasma filling for both the current NIF first quad experiment and for future experiments when the full NIF laser facility is used to heat hohlraums with 192 beams through two LEHs. The two curves are calculated using Eq. (6) assuming a minimum LEH radius of 0.3 mm, dictated by the minimum NIF laser spot size and a maximum angle of incidence of 50°. Extrapolating our analytic model predictions to full NIF hohlraum performance limits suggests a maximum achievable radiation temperature of T_{max} >700 eV.

4. Summary

First ICF related LPI and vacuum hohlraum experiments were performed on NIF. Laser propagation in ignition scale plasmas was measured demonstrating the necessity of laser beam smoothing by PS and SSD to avoid plasma filamentation and laser beam spraying. The first vacuum hohlraum experiments were used to activate Dante hohlraum drive diagnostics and to verify hohlraum drive scaling with laser power and hohlraum size. Models of extreme hohlraum plasma filling were corroborated in long pulse experiments and good agreement of thin wall imaging and Dante soft x-ray spectra with LASNEX simulations was obtained. As shown in Figure 10 peak internal Tr Dante measurements agreed well with LASNEX simulations including for a higher-temperature scale 3/8 hohlraum [ ] exceeding 300 eV. Analytical model used to estimate the radiation production limits is in good agreement with NIF measurements using four beams and can be used to predict hohlraum performance for full NIF with 192 beams.

*This work was performed under the auspices of the U.S. Department of Energy by the University of California, Lawrence Livermore National Laboratory under Contract No. W-7405-ENG-48.

References

[1] J.D. Lindl, Phys. Plasmas **2**, 3933 (1995).

[2] J.D. Lindl et al., Phys. Plasmas **11**, 339 (2004).

[3] L.J. Suter et al., Phys. Plasmas **3,** 2057 (1996).

[4] G.H. Miller, E.I. Moses and C.R. Wuest, Nucl. Fusion **44,** 228 (2004).

[5] S.H. Glenzer et al., Nucl. Fusion **44**, 185 (2004).

[6] J.A. Menapace, S.N. Dixit, F.Y. Genin, W.F. Brocious, Proc. Spie **5273**, 220 (2003).

[7] D. H. Munro, S. N. Dixit, A. B. Langdon, J. R. Murray, Appl. Opt. **43**, 6639 (2004).

[8] S.H. Glenzer et al., Phys. Rev. Lett. **80**, 2845 (1998).

[9] E. Dattolo et al., Phys. Plasmas **8**, 260 (2001).

[10] G.D. Tsakiris and R. Sigel, Phys. Rev. A **38**, 5769 (1988).

[11] B. Thomas, AWE, private communication, 1995

[12] E.L. Dewald, L.J. Suter, O.L. Landen et al., submitted to Phys. Rev. Letters 2005

[13] B. Remington et al., Metallurgical and Mat. Trans. A, **35A**, 2587 (2004).

[14] L.J. Suter et al., Rev. Sci. Instrum. **68**, 838 (1997).

[15] E.L. Dewald et al., Rev. Sci. Instrum. **75**, 3759 (2004).

[16] D. Froula et al., Rev. Sci. Instrum. **75**, 4168 (2004).

[17] A.J. Mackinnon et al., Rev. Sci. Instrum. **75**, 4183 (2004).

[18] J.W. McDonald et al., Rev. Sci. Instrum. **75**, 3753 (2004).

[20] R. Sigel et al., Phys. Rev. Lett. **65**, 587 (1990).

[21] G.B. Zimmerman and W.L. Kruer, Comm. Plasma Phys. Contr. Fusion **2**, 51 (1975).

[22] T.W. Johnston and J.M. Dawson, Phys. Fluids **16**, 722 (1973).

[23] R.W. Lee *et. al*., JQSRT **58,** 737 (1997).

[24] D. Hinkel et al., Phys. Plasmas, **12**, 056305 (2005).

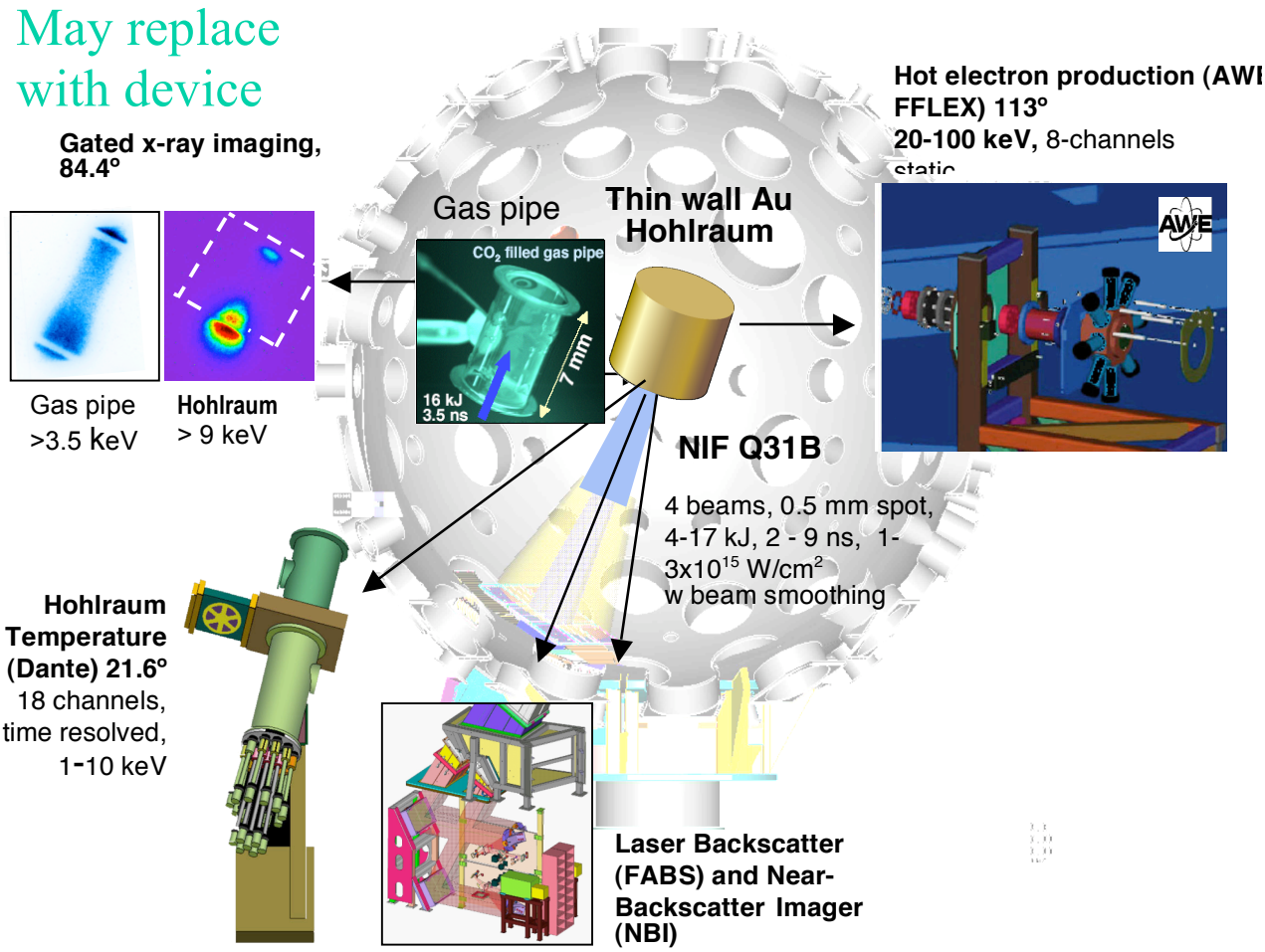

Figure 1 Experimental layout and diagnostics

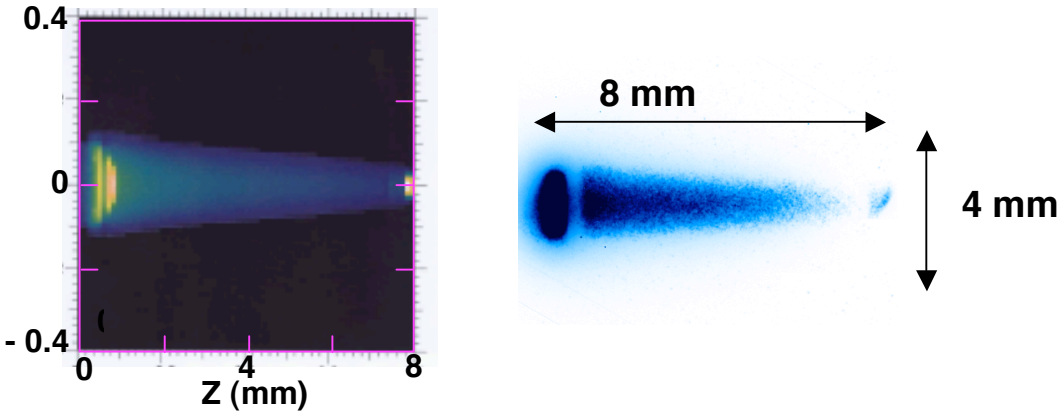

Figure 2

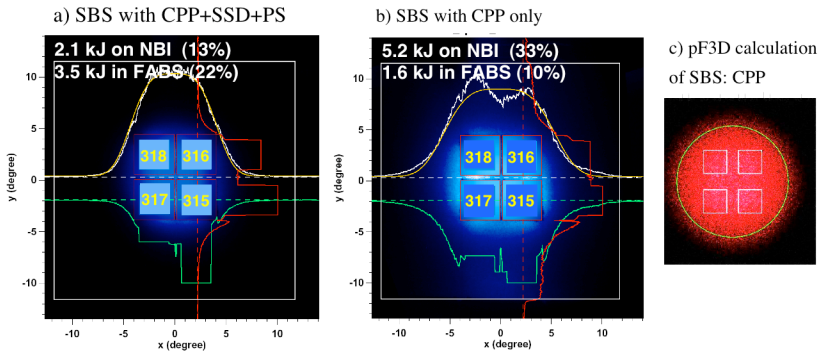

Figure 3 Stimulated Brillouin Laser backscattering measured with FABS and NBI for different beam conditioning: (a) with CPP, SSD and PS, (b) with CPP only; calculated SBS with pf3d with CPP only showing less beam spray than in the data

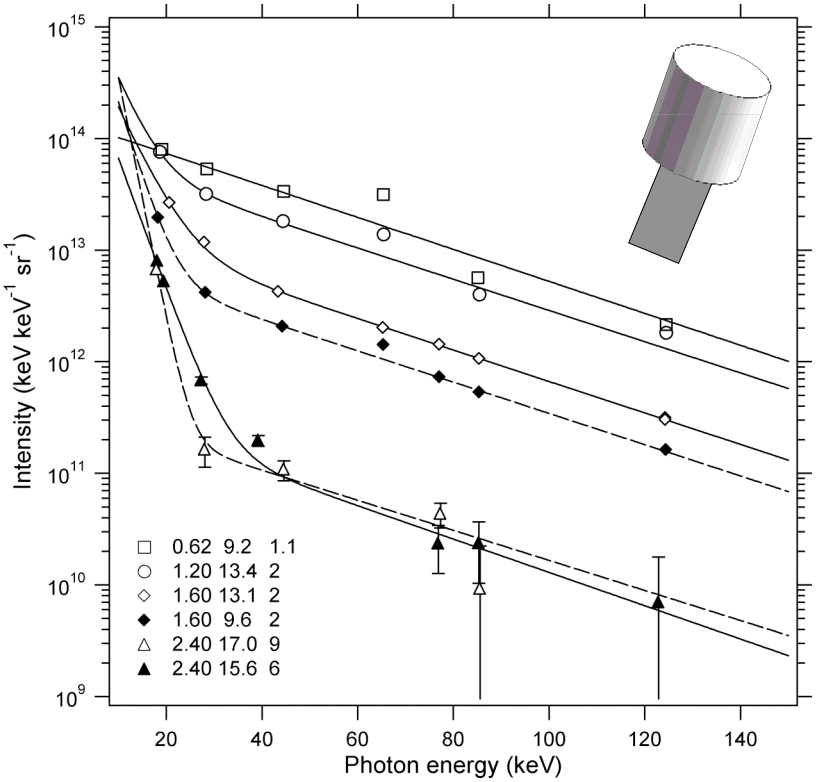
Intensity (keV keV^{-1} sr^{-1})
Photon energy (keV)
0.62 9.2 1.1
1.20 13.4 2
1.60 13.1 2
1.60 9.6 2
2.40 17.0 9
2.40 15.6 6

Figure 4

Figure 5 Spectra on the peak of the x-ray drive measured with Dante and simulated by LASNEX

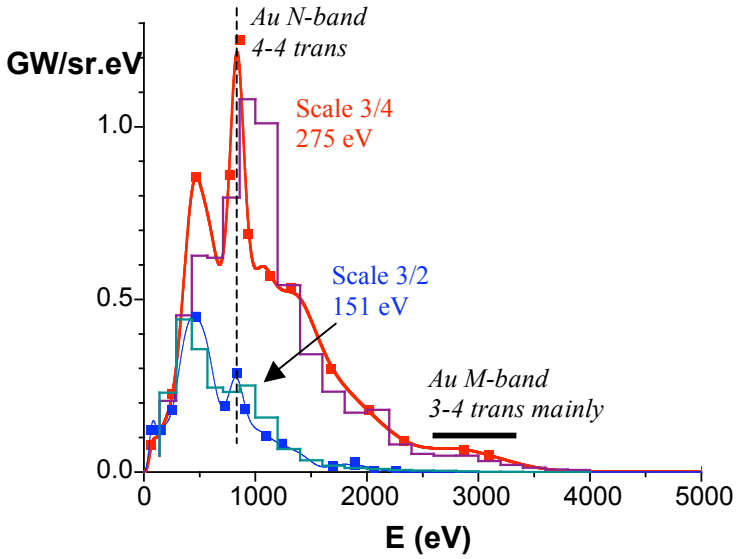

Figure 6

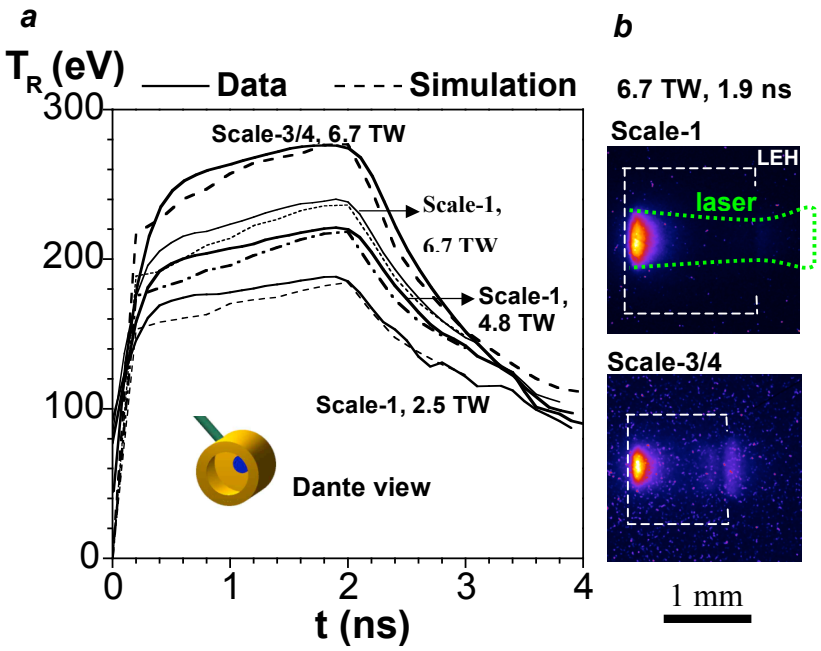
a
T_R (eV)
Data
Simulation
300
200
100
0
0
1
2
3
4
t (ns)
Scale-3/4, 6.7 TW
Scale-1, 6.7 TW
Scale-1, 4.8 TW
Scale-1, 2.5 TW
Dante view
b
6.7 TW, 1.9 ns
Scale-1
LEH
laser
Scale-3/4
1 mm

Figure 7

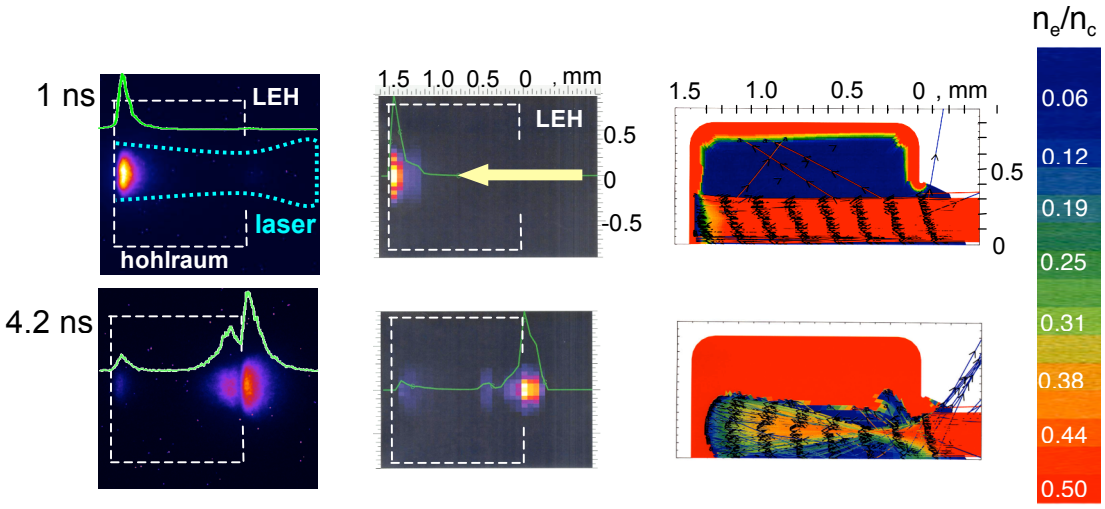
1 ns
LEH
laser
hohlraum
4.2 ns
1.5 1.0 0.5 0 , mm
LEH
0.5
0
-0.5
1.5 1.0 0.5 0 , mm
0.5
0
n_e/n_c
0.06
0.12
0.19
0.25
0.31
0.38
0.44
0.50

Figure 8

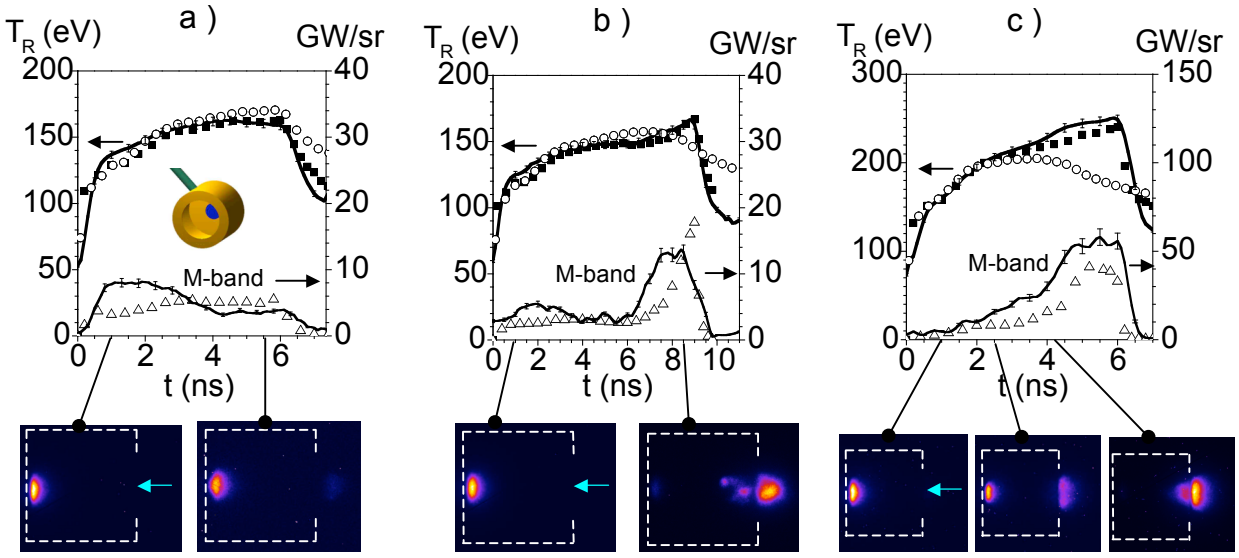

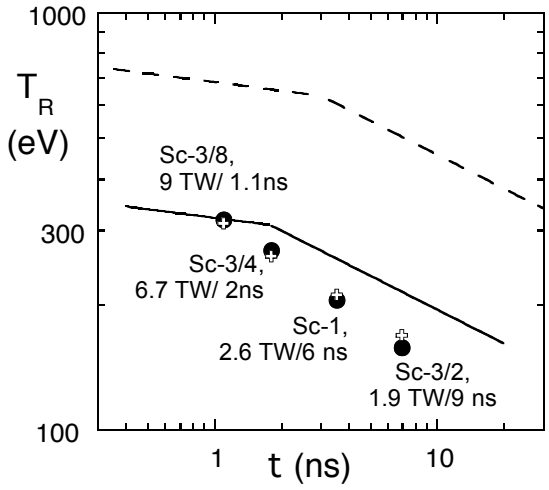
1000
300
100
T_R
(eV)
Sc-3/8,
9 TW/ 1.1ns
Sc-3/4,
6.7 TW/ 2ns
Sc-1,
2.6 TW/6 ns
Sc-3/2,
1.9 TW/9 ns
1
t (ns)
10

Figure 9

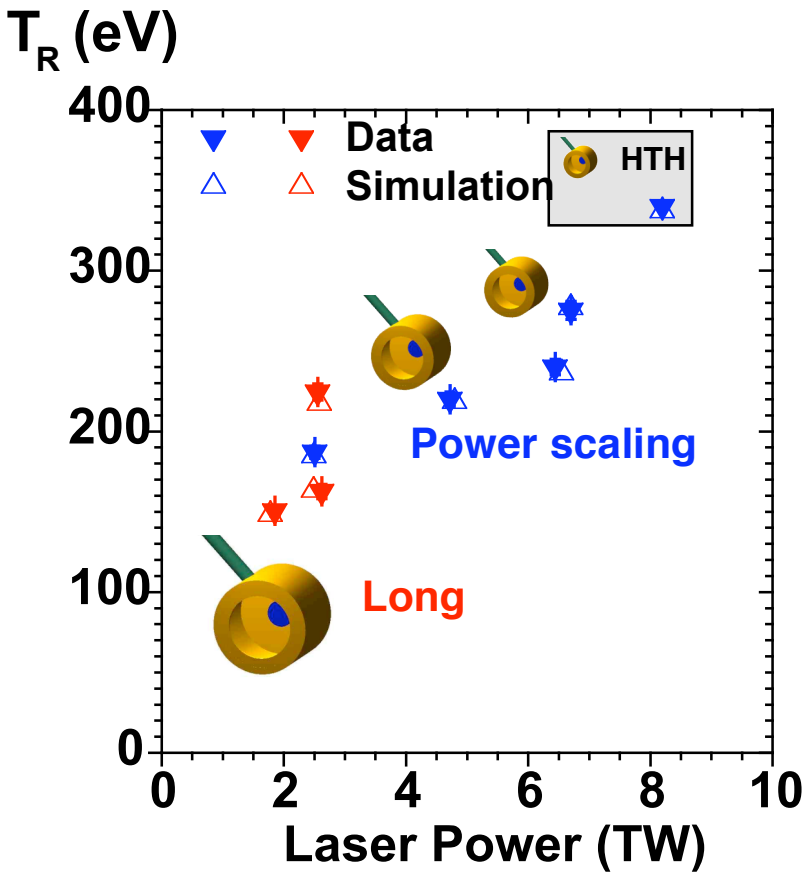

Figure 10

To be accurate, you should redraw each hohlraum with the right LEH size and spot size instead of shrinking